Project: Hydraulic significance and abstraction of the Excavation Damage Zone around borehole or tunnel openings

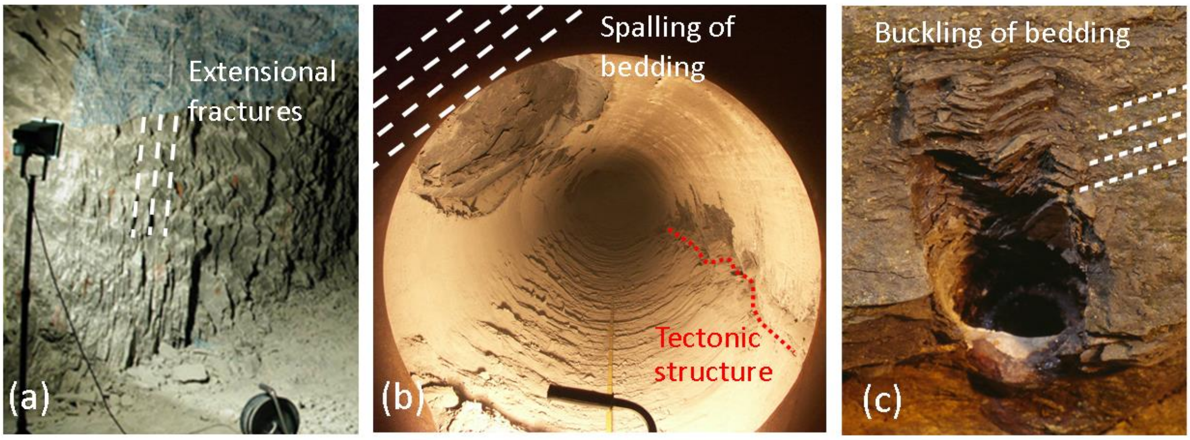

Excavation induced brittle features in Opalinus Clay (Mont Terri URL): (a) extensional fractures created during the excavation of Gallery 98 (Nagra 2002); (b) bedding related spalling processes in the crown of the HG-A microtunnel and interaction of stress controlled failure at the lower right side wall with a tectonic structure (Marschall et al. 2006); (c) buckling of the bedding planes around a small borehole (Blümling et al. 2007).

Employer:	Nagra
Tasks:	Development of an abstraction methodology of the Excavation Damage Zone; application to the HG-A experiment in Mont Terri
Model:	2D finite element model, time dependent hydraulic parameters
Software:	SUTRA

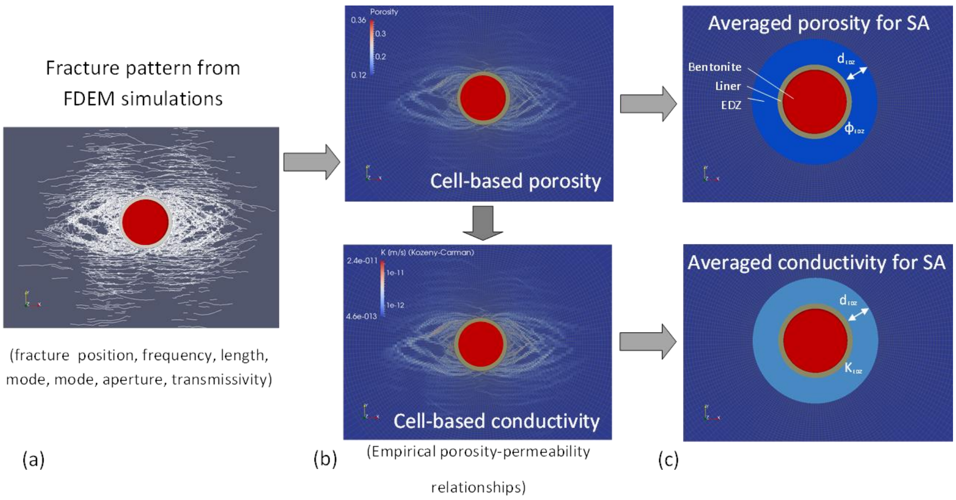

Concept of the EDZ abstraction process for Safety Assessment (SA) applicable for a circular tunnel. Read more below…

TK Consult AG

Hallenstrasse 10, CH-8008 Zürich
☎ +41(0)44 310 14 70
tkc@tkconsult.ch
http://www.tkconsult.ch

Summary

The Excavation Damaged Zone (EDZ) around the backfilled underground structures of a geological repository represents a possible release path for radionuclides and corrosion and degradation gases which needs to be addressed adequately in Safety Assessments (SA). The hydro-mechanical phenomena associated with the creation and temporal evolution of the EDZ are of sufficiently complex to preclude detailed representation of the EDZ in conventional SA modelling tools. Thus, simplified EDZ models, but able to mimic the safety relevant functional features of the EDZ, are required. In this context, TK Consult AG has developed a versatile and heuristic modelling approach with the goal of representing the creation and evolution of the EDZ in an abstracted and simplified manner. The key features addressed are the stochastic character of the excavation-induced fracture network and the self-sealing processes associated with the re-saturation after backfilling of the underground structures. The modelling approach has been tested on a range of generic repository settings in the context of a sensitivity study, aimed at investigating the impact of repository depth and in-situ stress conditions, amongst other factors, on the hydraulic significance of the EDZ after repository closure. Finally, the model has been benchmarked with a data set from an in-situ self-sealing experiment at the Mont Terri Underground Rock Laboratory (URL), demonstrating the ability of the modelling approach to mimic the evolution of hydraulic significance of the EDZ around a backfilled tunnel section during the re-saturation phase.

Introduction

At the Cluster Conference in Luxembourg (November 2003) on the "Impact of the Excavation Disturbed or Damaged zone (EDZ) on the performance of radioactive waste geological repositories", a general definition of the EDZ around underground excavations was agreed by the scientific community (Tsang *et al*. 2005): "The Excavation damaged zone (EDZ) is a zone with significant irreversible processes and significant changes in flow and transport properties. These changes, for example, can include one or more orders of magnitude increase in flow permeability". In recent years, the EDZ has been a focus of continuous international research activities, covering the key processes, phenomena and features associated with the creation and evolution of the EDZ for a variety of host rock formations, including crystalline rock, rock salt, soft clays and indurated clays (Alheid *et al*. 2007, Aranyossy *et al*. 2007). Soft clays and indurated clay formations were identified as a class of sedimentary rocks with a distinctive deformation behaviour, displaying transitional features between ductile yielding and brittle failure in response to the excavation process. In the context of radioactive waste disposal, special emphasis has been given to the favourable capacity of EDZ fractures to self-seal after closure of the backfilled repository structures (Bernier *et al*. 2007, Blümling *et al*. 2007, Bock *et al*. 2010).

The Opalinus Clay, an indurated clay formation in the Molasse Basin of Northern Switzerland, has been identified as a candidate host rock for a geological repository for radioactive waste in Switzerland. The EDZ around excavated openings in the Opalinus Clay formation is predominantly a zone of brittle failure, as confirmed by multiple evidences gained during construction of motor- and railway tunnels (e.g., Steiner *et al.* 2010). In the long-term, the fractures forming the EDZ are expected to re-seal in response to the re-saturation process and the corresponding pore pressure recovery.

Hallenstrasse 10, CH-8008 Zürich
☎ +41(0)44 310 14 70
tkc@tkconsult.ch
http://www.tkconsult.ch

Quantitative analyses in support of the assessment of long-term radiological safety of geological repositories are often based upon simplified representations of the EDZ, assuming a configuration of concentric shells (single shell or double shell, respectively) with enhanced hydraulic conductivity. The radius of the shell representing the EDZ typically depends on the tunnel radius and on the orientation of the tunnel axis with respect to the principal horizontal stress direction (e.g., Nagra 2002). Various numerical EDZ abstraction approaches have been proposed in recent years, from complex EDZ fracture networks to simplified representations with equivalent flow and transport characteristics. Lanyon & Senger (2011) developed a sequential modelling approach for indurated clay formations, based on a stochastic representation of the EDZ in terms of Discrete Fracture Network (DFN) models. The underlying hydraulic DFN models with stochastic distributions of fracture frequency, orientation and transmissivity were converted into Equivalent Porous Medium (EPM) models with stochastic permeability distribution using the approach suggested by Jackson *et al*. (2000). Combined water and gas flow along stochastic realizations of the EDZ was simulated with the EPM models. Eventually, effective properties suitable for performance assessment were derived by inverse modelling of the results of stochastic modelling with a simple single shell representation of the EDZ. Hawkins *et al*. (2011) presented a similar approach with applications to the Meuse / Haute Marne URL in the Callovo-Oxfordian formation in the North-Eastern Paris Basin.

Conceptual framework

Empirical and experimental evidence

When a geological repository is constructed in an indurated clay formation, the host rock around the newly created openings is expected to respond in a brittle manner. Part of the irreversible deformation already occurs as pre-deformation ahead of the tunnel face (Martin 1997; Yong 2008), whereas the development of the system of excavation-induced fractures continues during the excavation process and even after completion of the permanent tunnel support system. The shape and extension of the EDZ around the openings is controlled by many factors, including the general geological setting (e.g., rock mass strength, stress and pore pressure distribution, sedimentary and tectonic features, in-situ stress field), engineering design (e.g., configuration of the underground structures, excavation technique, support system / lining) and the impacts related to the operational phase (e.g., ventilation, waste emplacement). Rock deformation is complicated by clay-specific hydro-mechanical couplings, giving rise to long-lasting time-dependent processes in the EDZ even after closure of the backfilled repository structures. A typical inventory of discrete EDZ features consists of extensional fractures (Fig. 1a), caused directly by the short-term excavation-induced unloading (undrained elasto-plastic response), spalling and buckling of the bedding planes (Figs 1b and c), interactions with the existing tectonic features (Fig. 1b) and bounding shear-bands. These features delimit the EDZ and the intact rock zones (Blümling *et al*. 2007). Further EDZ features can be attributed to the operational phase, such as desiccation cracks in response to tunnel ventilation and swelling-induced disaggregation of the rock matrix, when subjected to water-based fluids (e.g., cement water during construction of the invert).

Hallenstrasse 10, CH-8008 Zürich
☎ +41(0)44 310 14 70
tkc@tkconsult.ch
http://www.tkconsult.ch

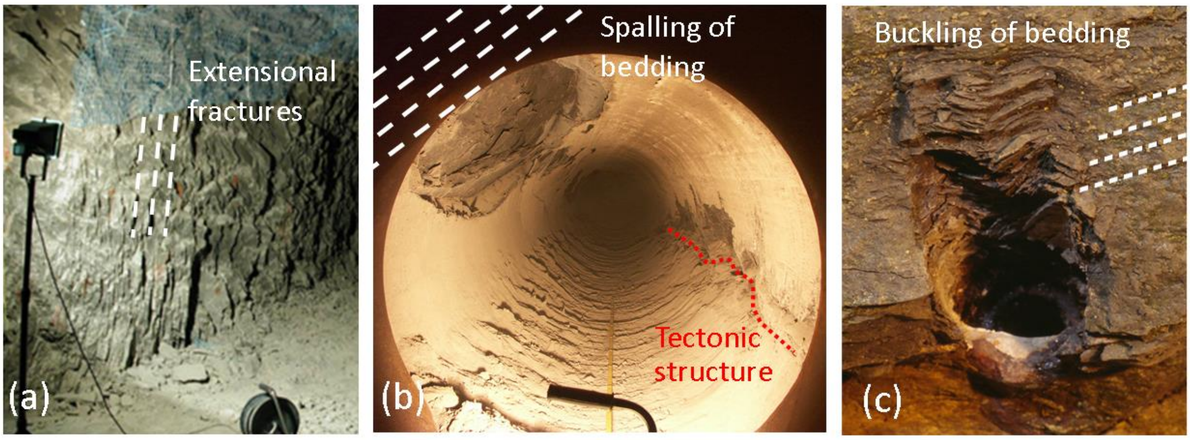

Fig. 1. Excavation induced brittle features in Opalinus Clay (Mont Terri URL): (**a**) extensional fractures created during the excavation of Gallery 98 (Nagra 2002); (**b**) bedding related spalling processes in the crown of the HG-A microtunnel and interaction of stress controlled failure at the lower right side wall with a tectonic structure (Marschall *et al*. 2006); (**c**) buckling of the bedding planes around a small borehole (Blümling *et al*. 2007).

The characterization of structural and hydro-mechanical features and processes of the EDZ has been a key research topic in the scientific programme of the Mont Terri URL in Switzerland. Early work by Martin & Lanyon (2003) and Corkum & Martin (2007) focused on the EDZ around tunnel sections normal to bedding strike, drawing on previous work from Bossart *et al*. (2002). More recently, emphasis was given to excavations parallel to bedding because these configurations are more relevant to a future deep repository (Marschall *et al*. 2006; Lanyon *et al*. 2014; Lisjak *et al*. 2015a). The impact of pre-existing tectonic features in the development of the EDZ was highlighted by Yong (2008) and Nussbaum *et al*. (2011). Yong reported a comparison of fracture density in boreholes around tunnels and niches at Mont Terri using data from over 100 boreholes (Fig. 2a). All structures other than those clearly related to tectonic features or drill core handing were counted over 0.5 m intervals. Almost 75% of the boreholes were drilled into the side-walls and data were normalized per borehole to reduce the bias. Fracture count in the first 0.5 m can be as high as 10 (with a mean spacing 5 cm) around some excavations, but typically reduces to less than 2 at 3 m from the tunnel wall.

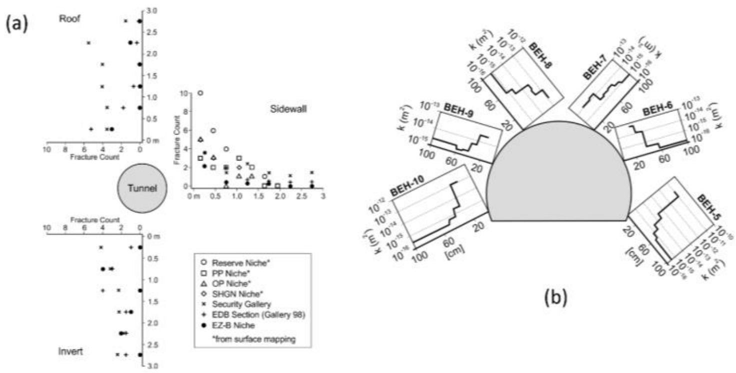

Fig. 2. Structural and hydraulic characterisation of the EDZ features around excavations in the Mont Terri URL: (**a**) fracture counts in 0.5 m borehole intervals from around the EZ-B Niche and previous sub-parallel excavations (modified from Yong 2008); (**b**) In situ permeability measurements conducted in Mont Terri experimental drift (from Bossart & Thury 2008).

Hallenstrasse 10, CH-8008 Zürich
☎ +41(0)44 310 14 70
tkc@tkconsult.ch
http://www.tkconsult.ch

At Mont Terri, small-scale in-situ permeability measurements in the EDZ were carried out in boreholes equipped with multi-packer systems oriented radial to the drift, isolating measurement intervals of 10 to 50 cm at various distances from the wall. Hydraulic pulse and constant head tests were carried out in the saturated part of the EDZ, whereas simple pneumatic tests were undertaken in the unsaturated rock in the immediate vicinity of the tunnel surface to investigate the local effective permeability (Bossart & Thury 2008). Figure 2b shows that permeability increases several orders of magnitude (up to 6-7) within 20 to 40 cm from the tunnel. This zone coincides with that exhibiting high fracture density.

Ferrari *et al*. (2013) and Romero & Gomez (2013) performed permeability tests in oedometric cells and triaxial cells on core samples from Mont Terri and from other locations in Northern Switzerland to investigate the stress dependence of permeability and porosity of intact Opalinus Clay. A consistent trend in porosity and permeability reduction with increasing effective stress was observed, although each sample shows the influence of preconsolidation and mineralogy. Hydraulic conductivity is typically below 10^{-13} m/s for effective stresses greater than 20 MPa and reduces further to ~ 10^{-14} at 100 MPa (Fig. 3a). Clay content, porosity and specific surface data obtained from the laboratory analysis of Opalinus Clay samples have been used to infer matrix hydraulic conductivity based on the Kozeny-Carman relationship (Alcolea *et al*. 2014).

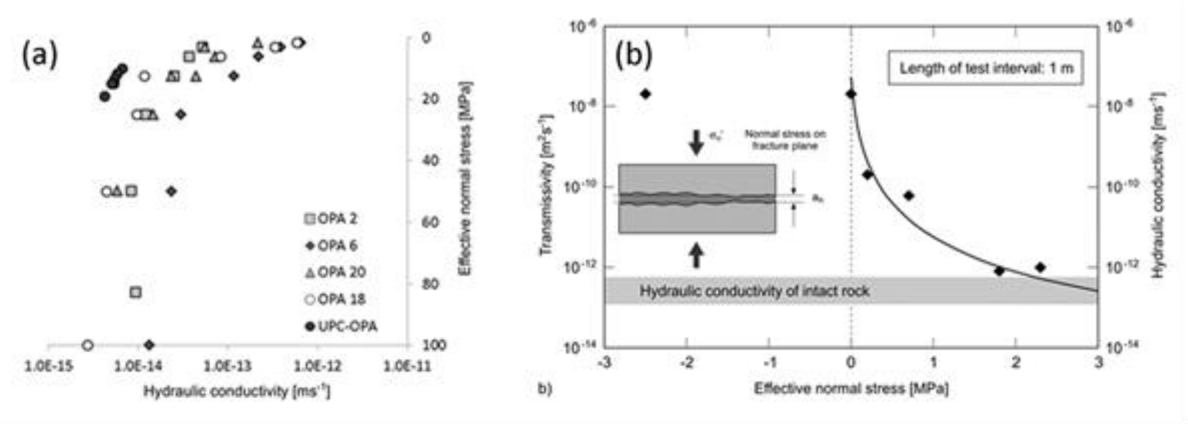

Fig. 3. Empirical relationships between stress and of hydraulic properties of the host rock: (**a**) stress-permeability relationship of the intact rock matrix and (**b**) hyperbolic transmissivity stress relationship between fracture transmissivity and normal effective stress (from Nagra 2004).

The dependence of fracture transmissivity on normal effective stress has been the issue of laboratory studies and in-situ tests (Blümling et al. 2007). As part of the GS experiment at Mont Terri, hydraulic tests were performed in a borehole before and after a hydrofrac experiment. Testing was conducted in a test interval containing a hydrofrac with a well-defined fracture geometry. Interval transmissivity increased by 5 to 6 orders of magnitude when the injection pressure exceeded the normal stress on the fracture plane (Fig. 3b). For low injection pressures, however, the interval transmissivity was close to that of the intact rock (T ≤ 10-12 m2/s). These findings can be explained by the dependence of fracture transmissivity (or hydraulic conductivity) on effective normal stress, which follows a hyperbolic fracture closure law (see Nagra 2004). An effective

Hallenstrasse 10, CH-8008 Zürich
☎ +41(0)44 310 14 70
tkc@tkconsult.ch
http://www.tkconsult.ch

mechanical self-sealing of the artificial fracture is observed already at moderate effective normal stresses in the order of 1 – 2 MPa (Fig. 3b).

Further experimental evidence on the self-sealing capacity of excavation-induced fractures has been gained by in-situ experiments at the Mont Terri URL, namely the SF experiment (Bernier et al. 2007) and the HG-A experiment (Lanyon et al. 2014). Notably, the long-term self-sealing tests in the HG-A microtunnel (Fig. 1b) served as a benchmark case for the modelling approach suggested in this work.

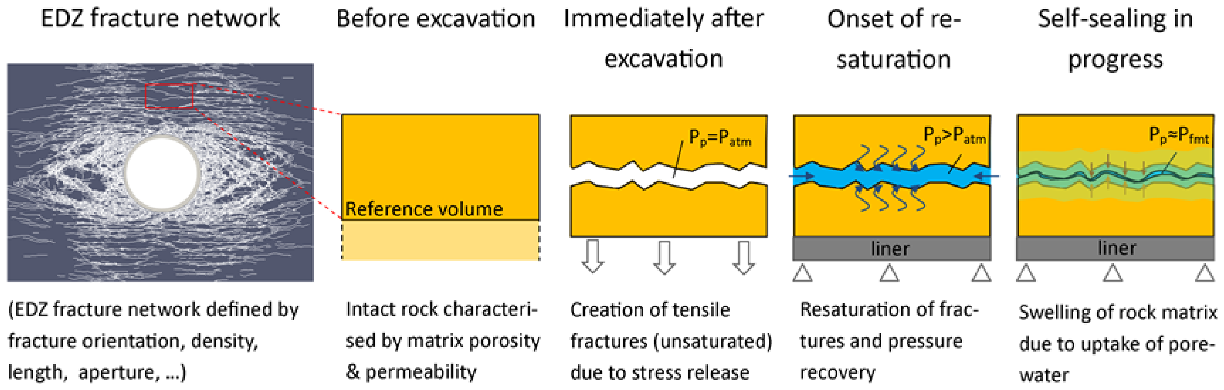

Fig. 4. Schematic sketch of the conceptual framework for EDZ fracture closure in Opalinus Clay, covering the key phenomena and features from the early post excavation phase until static formation pressure recovery.

Conceptualisation of fracture self-sealing

Drawing on the presented empirical and experimental evidence about the hydraulic significance of the EDZ during tunnel construction, its evolution during the operational phase and after backfilling of the underground structures, the functional requirements associated with a quantitative EDZ closure model can be formulated as follows (Fig. 4):

- The creation of the EDZ is a brittle process, i.e., the increase of the void volume in the damaged rock zone around the excavation is solely attributed to fracture opening, whereas the porosity of non-fractured rock remains essentially unchanged during the early times after excavation.

- Initially, the newly created EDZ fractures are unsaturated and exposed to atmospheric pressure, whereas the non-fractured rock remains saturated and exhibits high matrix suction as a consequence of the high gas entry pressure of the Opalinus Clay. The initial transmissivity of the unsaturated EDZ fractures is controlled by the fracture aperture and can be very high. The matrix conductivity remains essentially unchanged, i.e., it is the same as the conductivity of the intact rock.

- With time, the matric suction in the rock matrix decreases due to the uptake of pore water from outer rock zones and the fractures start to resaturate.

- Porewater uptake of the non-fractured rock zones is associated with swelling and consequently with an increase of matrix porosity. This porosity increase of the rock matrix occurs at the expense of fracture aperture, i.e., the fractures start to close and fracture transmissivity reduces drastically, whereas the hydraulic conductivity of the non-fractured matrix zones increases slightly as a consequence of the porosity increase.

- This increase of matrix porosity and hydraulic conductivity is associated with the decrease of fracture aperture and transmissivity, and progresses until the equilibrium of effective stresses is reached. This is essentially the case, when pore pressure reaches the static formation pressure.

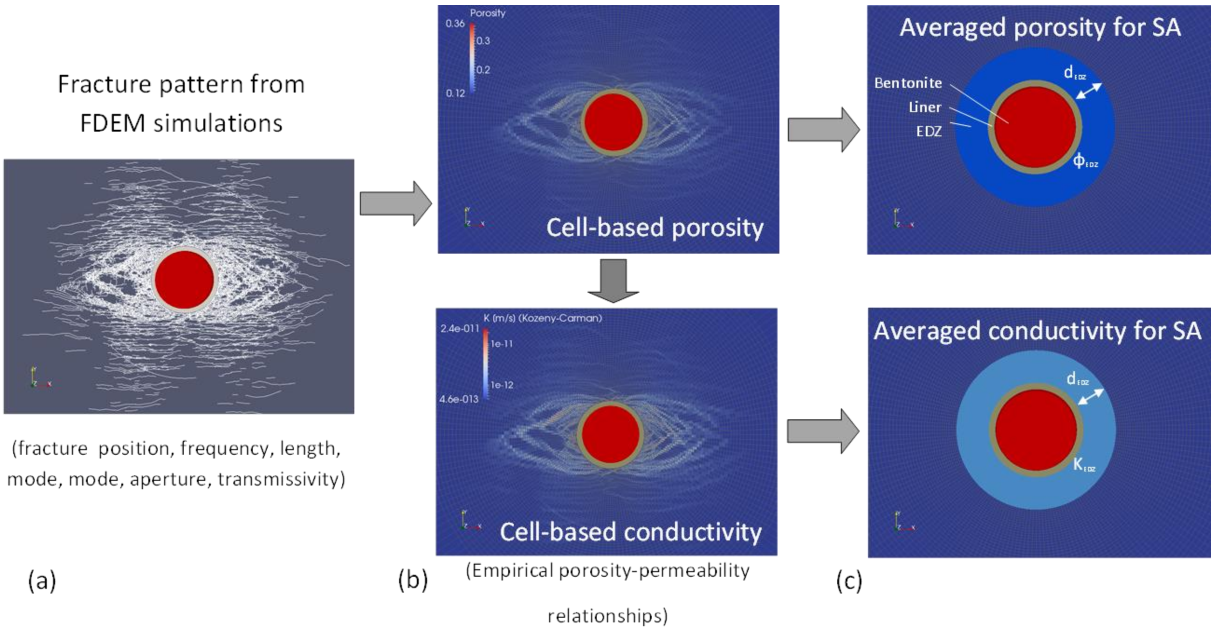

Fig. 5. Concept of the EDZ abstraction process for Safety Assessment (SA) applicable for a circular tunnel: (**a**) Representative fracture patterns are simulated for relevant repository configurations with a discrete element model (FDEM); (**b**) The discrete fracture patterns are converted in heterogeneous porosity and conductivity distributions; (**c**) In a final abstraction process, the heterogeneous porosity / conductivity distributions are converted in a shell defined by a radius and homogeneous porosity / conductivity.

A numerical approach for modelling the hydraulic significance of the EDZ is developed in the next section with the following goals: (i) to cope with a wide range of geological, hydrogeological and geomechanical conditions relevant to the candidate siting regions for a geological repository in Northern Switzerland, (ii) to cover the relevant hydraulic and geomechanical phenomena and processes associated with the creation of the EDZ during construction and its evolution during operational times and after backfilling of the underground structures, and (iii) to capture in a consistent way the experimental evidence of the EDZ self-sealing, which has been gained as part of in-situ experiments in underground rock laboratories (e.g., the HG-A experiment at Mont Terri). The methodology presented here consists of three main steps carried out sequentially (Fig. 5). First, a hybrid finite/discrete element method (FDEM; Geomechanica 2013 and 2014; Lisjak *et al.* 2015a and b) is used to simulate the geometry and geomechanical conditions of the discrete fracture networks forming the EDZ (Fig. 5a). The FDEM simulations are purely mechanical and mimic the excavation and emplacement processes. Second, the geometrical properties simulated by the FDEM are mapped onto a finite element mesh (Fig. 5b), which allows to solve the fluid motion equations in the excavation near-field. A salient feature of the suggested methodology is that hydraulic parameters of both fracture and matrix evolve with time as a response to re-saturation of the tunnel surroundings. Finally, an abstraction of the complex model is made based on the late time behaviour (after full re-saturation) of the system (Fig. 5c). The main outputs of the model are the spatio-temporal distributions of hydraulic parameters and the corresponding specific fluxes towards the tunnel, with special emphasis on the late time behaviour. Finally, the abstraction of the EDZ is implemented by defining a piece-wise homogeneous "shell-like" model with hydraulic behaviour identical to that of the complex model.

The present study focuses on the temporal evolution of hydraulic parameters of the EDZ around the tunnel. For illustration purposes, the methodology is applied to the HG-A experiment at the Mont Terri URL.

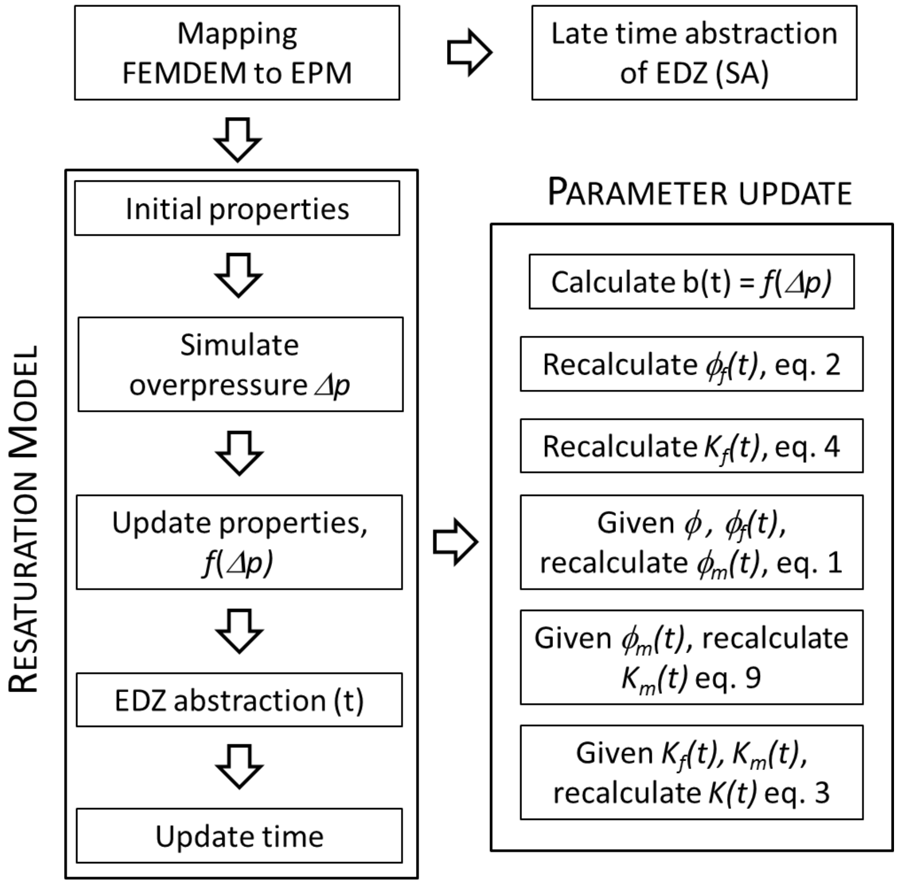

Fig. 6. Suggested modelling approach. The starting point is a mechanical simulation of the EDZ after excavation. Geometrical properties of the fractures delineating the EDZ are mapped to a continuum model. After mapping, and assuming that all fractures are closed (i.e., attributed with a residual aperture / irreducible transmissivity), the late time behaviour of the EDZ (t > 10'000 years) is analysed and an abstraction consisting of a piece-wise homogeneous model is proposed. Such abstraction is amenable to SA analysis. In addition, the temporal evolution of the EDZ during re-saturation can also be addressed by the continuum model. A decoupled hydro-mechanical model is posed, that updates fracture aperture at each time step as a function of overpressure (i.e., above atmospheric pressure). Hydraulic properties of the EDZ vary in time in response to re-saturation. The EDZ abstraction can therefore be made at intermediate times of re-saturation. In the insets, t denotes time, b is aperture, K is hydraulic conductivity and ϕ is porosity. Sub-indexes '*f*' and '*m*' denote fracture and matrix, respectively.

Modelling approach

Following Lanyon & Senger (2011), an EPM representing a cross-section orthogonal to the axis of the underground structure is used to model the re-saturation of the EDZ. Re-saturation leads to the self-sealing of the EDZ caused by mechanical closure of fractures and swelling of the clay rich minerals of the rock matrix. The modelling approach consists of three basic tools (Fig. 6): (1) mapping of FDEM geometrical properties, (2) re-saturation model, which calculates the pressure state of the system at a certain re-saturation stage and updates FDEM parameters accordingly and (3) EDZ abstraction. These tools are described in detail below and applied to an illustrative example.

Mapping of the FDEM to an equivalent continuum model

The fluid flow caused by the re-saturation of the EDZ is predominantly radial due to the shape of the EDZ and of the underground structure. Therefore, a radial finite element mesh is used, thus helping to alleviate the numerical artifacts caused by structured meshes while solving radial flow and to reduce the computational time. A zonation of hydraulic parameters is also adopted to assign different properties to different materials (Table 1). The mesh is finer at the zone encompassing the EDZ. Cell size increases according to a geometric progression. Hydraulic properties at cells are calculated from geometrical properties of the FDEM. To this end, the properties of fractures intersecting each cell (if any) are upscaled.

Cell porosity is calculated as:

$$\phi = \frac{V_p}{V_{tot}} = \frac{V_{p,f}(t) + \left(1 - \frac{V_{p,f}(t)}{V_{tot}}\right) V_{p,m}(t)}{V_{tot}} = \phi_f(t)\big(1 - \phi_m(t)\big) + \phi_m(t) \qquad (1)$$

where ϕ [-] is total porosity, V_p and V_{tot} [L^3] are the void volume and total volume of the cell, respectively and t [T] is time. Note that we work per unit length in the axial direction of the tunnel. Therefore, cell volumes are equivalent to cell areas. Subscripts *'f'* and *'m'* refer to fracture and matrix, respectively. Constant deterministic values of matrix porosity for the different materials defining the model zonation are summarized in Table 1.

Fracture porosity of a given cell is calculated as an average of the geometric parameters defining the fractures intersecting the cell:

$$\phi_f^j(t) = \frac{\sum_i b_i(t) L_i^j}{V_j} \qquad (2)$$

where b_i [L] and L_i^j [L] are the aperture and trace length of fracture *'i'* intersecting cell *'j'*. V_j is the cell volume (area).

Hallenstrasse 10, CH-8008 Zürich
☎ +41(0)44 310 14 70
tkc@tkconsult.ch
http://www.tkconsult.ch

Table 1. Model zonation and deterministic values of hydraulic properties. The canister, emplaced at the centre of the model is not simulated. Instead, a no flow boundary condition is set there. R_{model} denotes the radius of the outer boundary of the model.

Zone	~Radial extent (m)	Porosity	In-plane conductivity	
			Kxx **(m/s)**	***Kzz*** **(m/s)**
Canister	0 - 0.5	N.A.	N.A.	N.A.
Bentonite (buffer zone)	0 -1.25	0.35	10^{-13}	10^{-13}
Steel Liner	1.25-1.5	0.20	10^{-10}	10^{-10}
EDZ	Variable	Variable	Variable	Variable
Intact Opalinus Clay (far field)	R_{model}=120	0.12	10^{-13}	$2\cdot10^{-14}$

Hydraulic conductivity of a cell K [LT^{-1}] is calculated as:

$$K(t) = K_m(t) + K_f(t) \tag{3}$$

where K_m [LT^{-1}] denotes hydraulic conductivity of the matrix (Table 1) and K_f [LT^{-1}] is fracture conductivity of cells intersected by fractures (0 otherwise). K_f is calculated from fracture trace length and transmissivity, calculated from fracture aperture using a cubic law approximation:

$$K_f^j = \frac{\sum_i T_i(t) L_i^j}{V_j} \quad ; T_i = \frac{\rho g b(t)_i^3}{12\mu} \tag{4}$$

where T_i [L^2T^{-1}] is the transmissivity of fracture *'i'* intersecting cell *'j'*, g is gravity [L^2T^{-1}] and ρ [ML^{-3}] and μ [$ML^{-1}T^{-1}$] the fluid density and dynamic viscosity, respectively.

Within the modelled cross section, the flow takes place mainly in the fracture plane (i.e., along its longest edge). Thus, anisotropic hydraulic conductivities are calculated from the maximum conductivity by standard projection:

$$\begin{aligned} K_{f,xx}(t) &= K_f(t)\cos\theta \\ K_{f,zz}(t) &= K_f(t)\sin\theta \end{aligned} \tag{5}$$

where θ is the inclination of the fracture measured counter-clockwise from the positive x-axis.

Hydraulic conductivities in x and z directions are then calculated at each cell:

$$\begin{aligned} K_{xx}(t) &= K_{f,xx}(t) + K_{m,xx}(t) \\ K_{zz}(t) &= K_{f,zz}(t) + K_{m,zz}(t) \end{aligned} \tag{6}$$

Finally, cell conductivity K_{yy}, orthogonal to the cross section (i.e., parallel to the axis of the opening) is calculated as:

$$K_{yy}(t) = \sqrt{K_{xx}(t)\cdot K_{zz}(t)} \tag{7}$$

Hallenstrasse 10, CH-8008 Zürich
☎ +41(0)44 310 14 70
tkc@tkconsult.ch
http://www.tkconsult.ch

In equation 7, it is assumed that the cell size is sufficiently small and that the anisotropy of hydraulic conductivity is not significant. Note also that equations (1) and (3) involve time dependent hydraulic parameters. The way these parameters vary in time is described in the next section.

FDEM parameters at a certain re-saturation stage

The re-saturation of the system causes two effects. On the one hand, a pressure increase at the fractures from atmospheric to hydrostatic pressure condition causes a reduction of effective normal stresses. This reduction is assumed to be insufficient to either stimulate existing fractures (i.e., fracture trace length is constant) or to generate new fractures. Yet, the reduction of effective stresses leads to mechanical closure of fractures. Fracture closure leads to a reduction of fracture porosity and hydraulic conductivity, according to equations (2) and (4). On the other hand, the high percentage of clay minerals causes the matrix to swell at low pressure variations (<2 MPa). Swelling causes both matrix porosity and hydraulic conductivity to increase with time.

Drawing on previous analyses (Fig. 3b; see also Nagra 2004), fracture closure is accommodated in the model through a function relating fracture aperture and overpressure Δp [$ML^{-1}T^{-2}$] (i.e., pressure above atmospheric):

$$b(t) = b_0\left(1 - \frac{1}{\left(\frac{b_0 K_{n0}}{\Delta p(t)}\right)^{1-\alpha} + 1}\right) \qquad (8)$$

where b_0 is the initial fracture aperture (here, before the re-saturation starts, immediately after excavation and emplacement) and K_{n0} is fracture normal stiffness ($ML^{-2}T^{-2}$; ~920 MPa/m, Yong *et al.* 2010). The exponent α controls the velocity of fracture closure and is referred to as closure rate. Note that at early times ($\Delta p \rightarrow 0$), the aperture tends to the initial one, in the absence of pressure perturbations. Low α values lead to smaller apertures for a given value of overpressure (alternatively, of re-saturation time). Correspondingly, the time required for a full re-saturation of the system is smaller for small α values. α is estimated by assuming that, after full re-saturation, all fractures are closed and attributed with a residual aperture b_r = $8.9 \cdot 10^{-8}$ m, corresponding to an irreducible transmissivity $T_r = 5.7 \cdot 10^{-16}$ m^2/s according to the cubic law in equation 4. The residual aperture is selected in such a way that, after full re-saturation (i.e., $\Delta p \rightarrow$ 7.8MPa), the fracture hydraulic conductivity of the most conductive cell is small and equivalent to the matrix conductivity of the intact Opalinus Clay. This low residual transmissivity is in agreement with the results of the GS-experiment at Mont Terri (Nagra, 2004; Fig. 3b). Plugging Δp and b_r in equation (8) yields $\alpha \sim -3.4$.

Matrix porosity ϕ_m (t) is calculated from ϕ_f (t) by assuming that total porosity ϕ is constant along the re-saturation process (equation 1). This assumption can be justified by the fact that fracture porosity diminishes with time due to mechanical closure caused by reduction of effective stresses, whereas matrix porosity increases with time due to swelling of the rock matrix. The rates of porosity reduction/increase of ϕ_f (t) and ϕ_m (t) are highly unknown and therefore it is assumed for simplicity that the two effects cancel each other out. Matrix porosity and hydraulic conductivity are related through the well-known Kozeny-Carman equation:

$$K_m(t) = \frac{\phi_m(t)^3}{(1-\phi_m(t))^2} \cdot \frac{\rho \cdot g}{\mu} \cdot \frac{{d_{10}}^2}{180} \qquad (9)$$

where d_{10} [L] is the particle size for which 10% of the soil is finer. d_{10} is calculated upon the pair of porosity-hydraulic conductivity values of the intact Opalinus Clay in Table 1, resulting $d_{10}=1.94 \cdot 10^{-8}$ m.

The re-saturation process is simulated by a numerical model with the zonation and deterministic parameters in Table 1 and with the following boundary conditions: zero drawdown at the external boundary (i.e., the far field is not perturbed by the presence of the underground structure due to the low hydraulic conductivity of the intact Opalinus Clay) and zero flux at the inner zone representing the canister, assumed impervious for simplicity. The initial pressure condition is hydrostatic at cells not intersected by fractures. Otherwise, atmospheric pressure is imposed. At a given time t, the overpressure distribution is calculated and fracture apertures are recalculated according to equation (8). Fracture transmissivities are then calculated according to the cubic law in equation (4). Fracture porosity and hydraulic conductivity are then calculated according to equations (2) and (4).

Figures 7 and 8 display the temporal evolution of pressure and total hydraulic conductivity at selected times. Early stages of the re-saturation process are controlled by the high transmissivity of the many fractures defining the EDZ. This process is initially very fast, but very slow at mid and late times, when a certain degree of re-saturation is already achieved. Actually, the buffer zone (back-filled with bentonite) and some fractures are initially unsaturated. A set of bi-phase scoping simulations was carried out to address the impact of the initial unsaturated state. It was observed that the saturation of the initially unsaturated pores takes less than 10 years. This time frame is negligible compared to the total time required for the full re-saturation of the system (> 20’000 years). Therefore, the initial unsaturated state was ignored to decrease the overall computational time. The time at which full re-saturation occurs is highly uncertain and largely depends on the closure rate α. This issue is discussed later.

The temporal evolution of the system can be observed in Figure 9, which displays the number of closed fractures (i.e., attributed with the residual aperture) as a function of time. Most fractures are closed at early re-saturation times. This number steadily decreases with time and reaches a plateau after approximately 1’000 years. The number of fractures defining the EDZ is >43’000. However, the number of closed fractures at the end of the simulation period is ~37’000. This means that full re-saturation of the EDZ was not achieved. The fractures that remain open cluster around the tunnel and are those with largest initial aperture. The fast hydraulic response of the system is also observed in this plot.

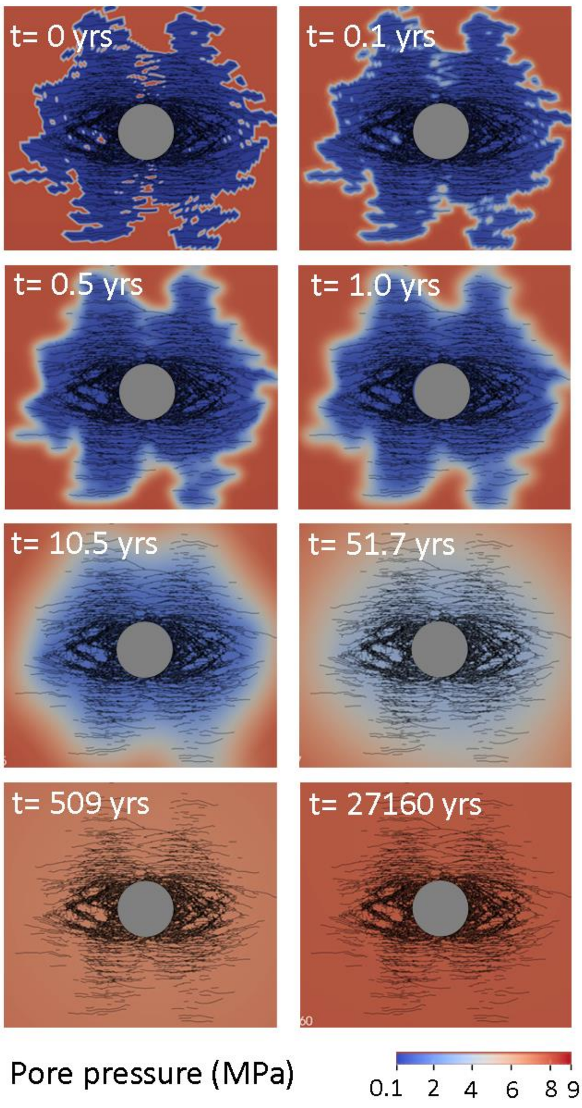

Fig. 7. Temporal evolution of pressure at selected time steps. Fractures defining the FDEM are superimposed (in black).

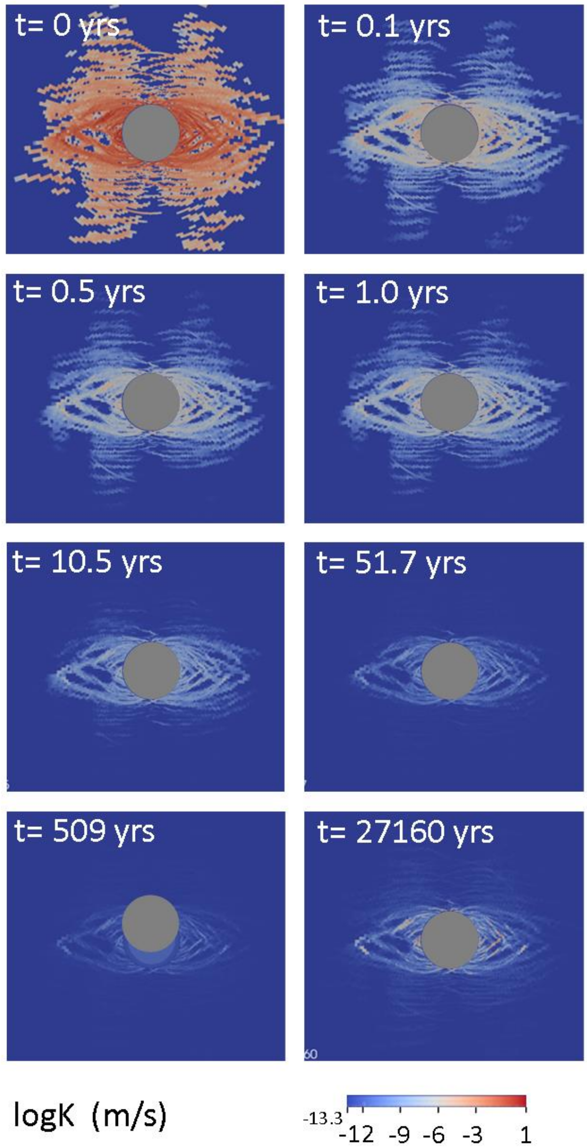

Fig. 8. Temporal evolution of axial hydraulic conductivity K_{yy} at selected time steps.

Abstraction of the EDZ

This section describes the methodology for the abstraction of the EDZ. The abstraction consists of a simple piece-wise homogeneous shell model including the buffer zone, the liner, an equivalent EDZ and the intact Opalinus Clay (i.e., the far field). Homogeneous hydraulic properties are assigned to each zone. Hydraulic properties of the EDZ are averaged over its extension. Such abstraction is amenable to SA and frees the modeller of the burden of having to deal with complex, heterogeneous, EDZ models. We consider the axial flow (i.e., parallel to the axis of the gallery) through the modelled section, calculated as:

$$Q_y(r_i) = \sum_{j \in shell,i} K_y^{i,j} A_{i,j} \quad (10)$$

where r_i [L] denotes the radius of a shell '*i*', '*j*' is a counter of cells defining that shell, $A_{i,j}$is the cell area and $K_y^{i,j}$ denotes axial hydraulic conductivity (equation 7). $Q_y(r_i)$ [L^3T^{-1}] is the axial flow rate under unit hydraulic head gradient between the extremes of the tunnel (i.e., the hydraulic conductance). To eliminate spurious mesh-related effects, Q_y is normalized by the area of the shell, thus becoming a specific flux q_y [LT^{-1}]. Under unit hydraulic head gradient conditions, the specific flux at a certain shell is the average of the axial hydraulic conductivity.

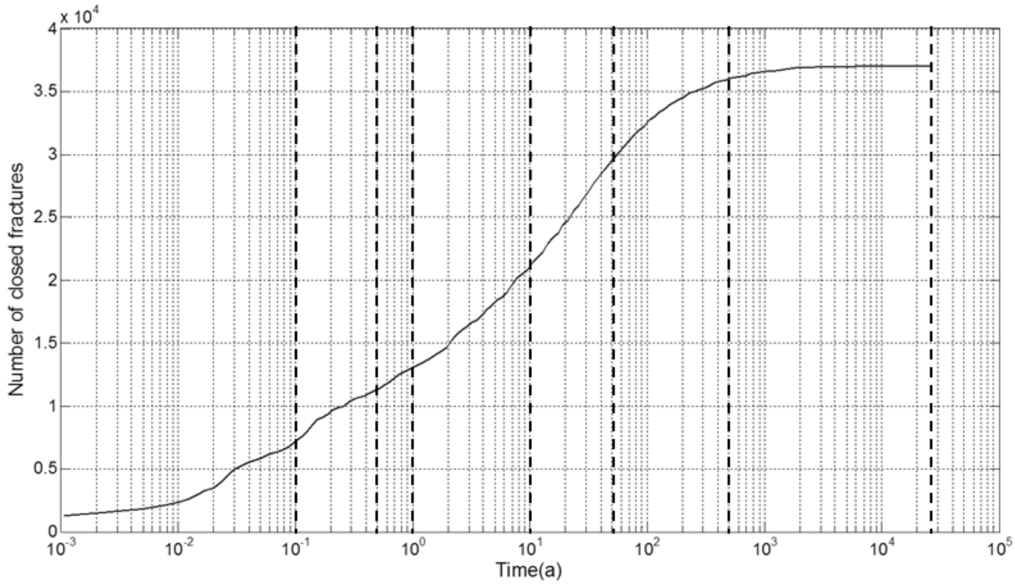

Fig. 9. Number of closed fractures vs time. The FDEM is made of 43'000 fractures. Vertical dashed lines depict the time steps in Figures 1 and 2.

Figure 10 depicts the temporal evolution of the equivalent EDZ hydraulic conductivity and of the flow rate across the abstracted EDZ Q_y. The equivalent hydraulic conductivity of the EDZ (or analogously, the total circulating flow rate) drops approximately by 11 orders of magnitude due to the mechanical closure of fractures and swelling of the clay rich materials of the rock matrix.

Relevant to SA are the axial fluxes and porosities at late times (i.e., after full re-saturation of the system, when all fractures are closed). Several observations can be made based on Figure 11:

- The specific flux q_y across fractures drops by almost 14 orders of magnitude after full re-saturation of the system (Fig. 11a) and by 13 orders of magnitude when the matrix is considered (Fig. 11b). Note that the total axial flux is already the residual one (~10^{-13} m/s) approximately 6 m far away from the centre of the opening, corresponding to the equivalent radius of the EDZ.

- At early times (Fig. 11c), fracture porosity decreases several orders of magnitude along a very small radial distance of ~6m (i.e., the equivalent radius of the EDZ).

Hallenstrasse 10, CH-8008 Zürich
☎ +41(0)44 310 14 70
tkc@tkconsult.ch
http://www.tkconsult.ch

Instead, matrix porosity is the original one because swelling of the rock matrix did not take place yet. At late times (Fig. 11d), fracture porosity is reduced ~4 orders of magnitude due to mechanical closure. Instead, matrix porosity increases and coincides with total porosity because all fractures are closed. In fact, there is no distinction between the red and black lines on Figure 11d.

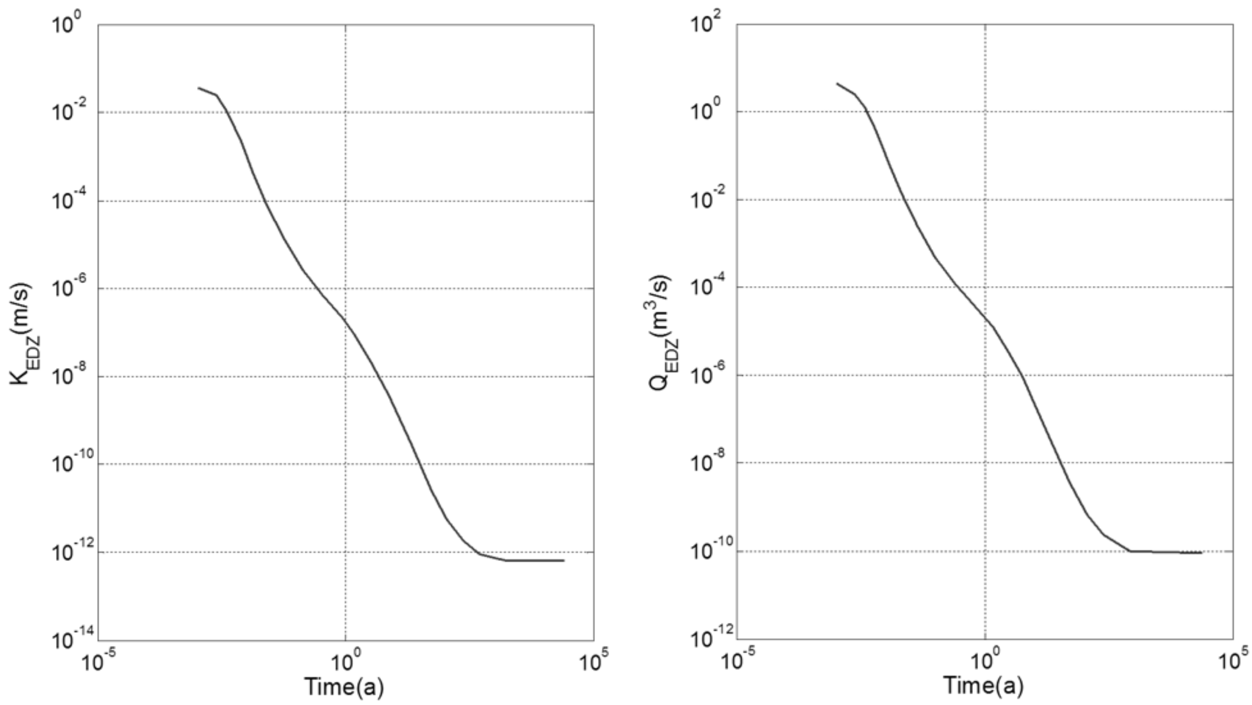

Fig. 10. Temporal evolution of (**a**) equivalent axial hydraulic conductivity of the EDZ and (**b**) axial flow rate.

The late time spatial distributions of effective porosity ϕ (r) and hydraulic conductivity K (r) are the subject of further analysis, given its relevance to SA. First, averaged profiles $<\phi$ (r)> and $<K$ (r)> are obtained at each shell of cells defining the mesh of the EPM. The arithmetic mean is adopted for the porosity profiles, whereas the geometric mean is used to estimate the averaged conductivity profiles. Second, the average values of void volume $<V_p>$ and total axial flux $<Q>$ are calculated by integration:

$$< V_p >= \int_{r_0}^{R_{max}} [\phi\,(\mathrm{r}) - \phi_m] \cdot r \cdot dr$$

$$< Q >= \int_{r_0}^{R_{max}} [K(\mathrm{r}) - K_m] \cdot r \cdot dr \qquad (11)$$

where r_0[L] and R_{model}[L] are the radius of the unlined gallery and of the modelled section, respectively. Third, $<V_p>$ and $<Q>$ are used to define homogenized properties of the abstracted EDZ in terms of a relationship between the EDZ equivalent porosity ϕ_{equiv}, hydraulic conductivity K_{equiv} and radius r_{equiv}:

$$\phi_{equiv} = \phi_m + \frac{< V_p >}{\pi \left(r_{equiv}^2 - r_0^2 \right)}$$
$$K_{equiv} = K_m + \frac{< Q >}{\pi \left(r_{equiv}^2 - r_0^2 \right)} \tag{12}$$

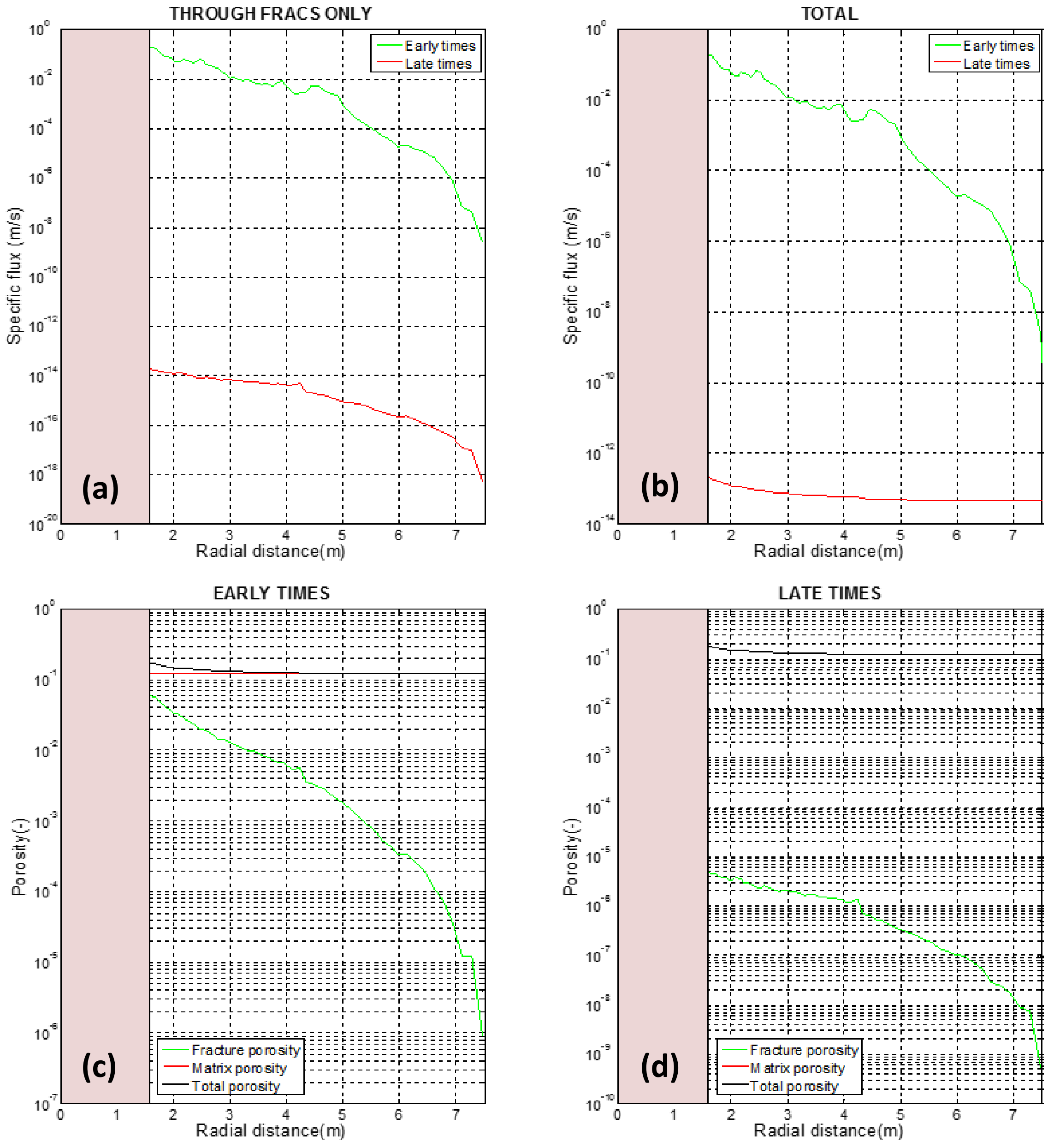

Fig. 11. Spatial distribution of: (**a**) specific axial flux q_y through EDZ fractures only at early and late times; (**b**) total specific axial flux at early and late times; (**c**) porosities at early times; (**d**) porosities at late times.

Sensitivity analysis

This section reports on the sensitivity analysis of the EDZ significance to various repository settings, relevant to a deep geological repository in the proposed siting regions in Northern Switzerland. Excavation-induced fracture patterns around the repository structures were simulated for repository depths between 450 and 800 m below ground, horizontal to vertical stress ratios Ko =Sh/Sv between 0.8 and 1.3 and rock mass strengths, varying by a factor 5 around the reference values, representative for the intact Opalinus Clay (Geomechanica 2013). Further simulations included stiff and soft tunnel support systems and hypothetical repository configurations like an intersecting fault system. A 3.0 m diameter circular opening for the high-level waste SF-HLW emplacement tunnel (HAA hereinafter) is analysed in this study. Fig. 12 displays simulated fracture patterns around the HAA cross section for different repository depths (650 and 800 m below ground), different stress ratios (Ko = 0.8, 1.0 and 1.3), different rock strengths (low, reference, high) and different stiffnesses of the tunnel support (rigid, reference, soft). Notably, the fracture patterns exhibit marked differences in terms of size, shape and fracture intensity.

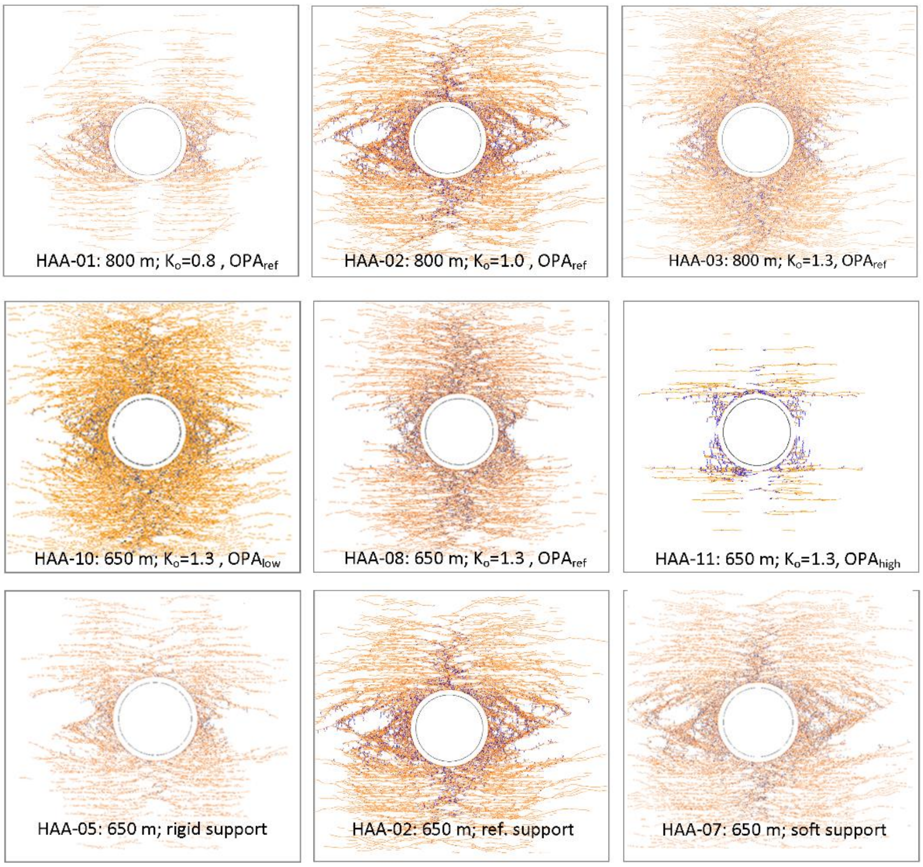

Fig. 12. EDZ fracture patterns around a circular SF/HLW emplacement tunnel ("HAA cross section") simulated for various repository settings. The sensitivity cases comprise the variation of repository depth, stress ratio $K_o = S_h/S_v$, rock strength (OPA_{low}=0.5 × reference strength, OPA_{ref}, OPA_{low}=3 × OPA_{ref}) and stiffness of tunnel support (stiff lining: core softening ratio γ=0.003; reference support: γ=0.01; soft lining γ=0.05). OPA denotes Opalinus Clay. Examples taken from Geomechanica (2013).

Alcolea et al. (2014) analysed the hydraulic behaviour of the EDZ at HAA cross sections and also considered larger openings like shafts. The cross sections of the HAA-models were assumed perpendicular to the strike of flat-lying bedding planes (i.e., HAA models are vertical sections). The effect of the tectonic imprint on the EDZ response was investigated using 5 variants of the HAA model, in which 3 deterministic fractures dipping at 80° intersect the back and invert of the gallery. These deterministic fractures have 10 cm thickness and are spaced 0.5 meters. Table 2 summarizes the main features of the simulations being analysed.

Table 2. Summary of HAA model simulations.

Model	S_v (MPa)	S_h (MPa)	Strength properties)	Elastic modulus of support (MPa)	Core softening ratio γ	Number of EDZ fractures	Average aperture (mm)	Average initial transmissivity (log10 m²/s)
Sensitivity to in-situ stress conditions and core softening ratio								
HAA-01	19.6	15.7				43058	0.40	-4.28
HAA-02	19.6	19.6			0.01	46366	0.40	-4.28
HAA-03	19.6	25.5				55543	0.43	-4.19
HAA-04	19.6	15.7				22419	0.30	-4.66
HAA-05	19.6	19.6	OPAx2	32	0.05	25237	0.31	-4.62
HAA-06	19.6	25.5				34891	0.36	-4.43
HAA-07	19.6	19.6			0.008	50411	0.41	-4.26
HAA-08	15.9	20.7			0.008	42331	0.41	-4.24
HAA-09	15.9	15.9			0.003	36658	0.45	-4.11
Sensitivity to strength parameters								
HAA-10			OPAx1.5			62413	0.37	-4.38
HAA-11	15.9	20.7	OPAx3	32	0.008	18492	0.51	-3.96
HAA-12			OPAx4			6697	0.68	-3.59
HAA-13			OPAx5			3363	0.84	-3.32
Sensitivity to the presence of faults								
HAA-14			OPAx2		0.01	56057	0.40	-4.28
HAA-15			OPAx1.5			85324	0.38	-4.34
HAA-16	19.6	19.6	OPAx3	32	0.008	25671	0.43	-4.20
HAA-17			OPAx4			15037	0.45	-4.12
HAA-18			OPAx5			9724	0.41	-4.26
Sensitivity to shotcrete stiffness								
HAA-19			OPAx2	16		42376	0.41	-4.24
HAA-20			OPAx2			43260	0.45	-4.13
HAA-21	15.9	20.7	OPAx1.5		0.008	65376	0.40	-4.27
HAA-22			OPAx3	3.2		19994	0.55	-3.86
HAA-23			OPAx4			7378	0.71	-3.54
HAA-24			OPAx5			3487	0.85	-3.30

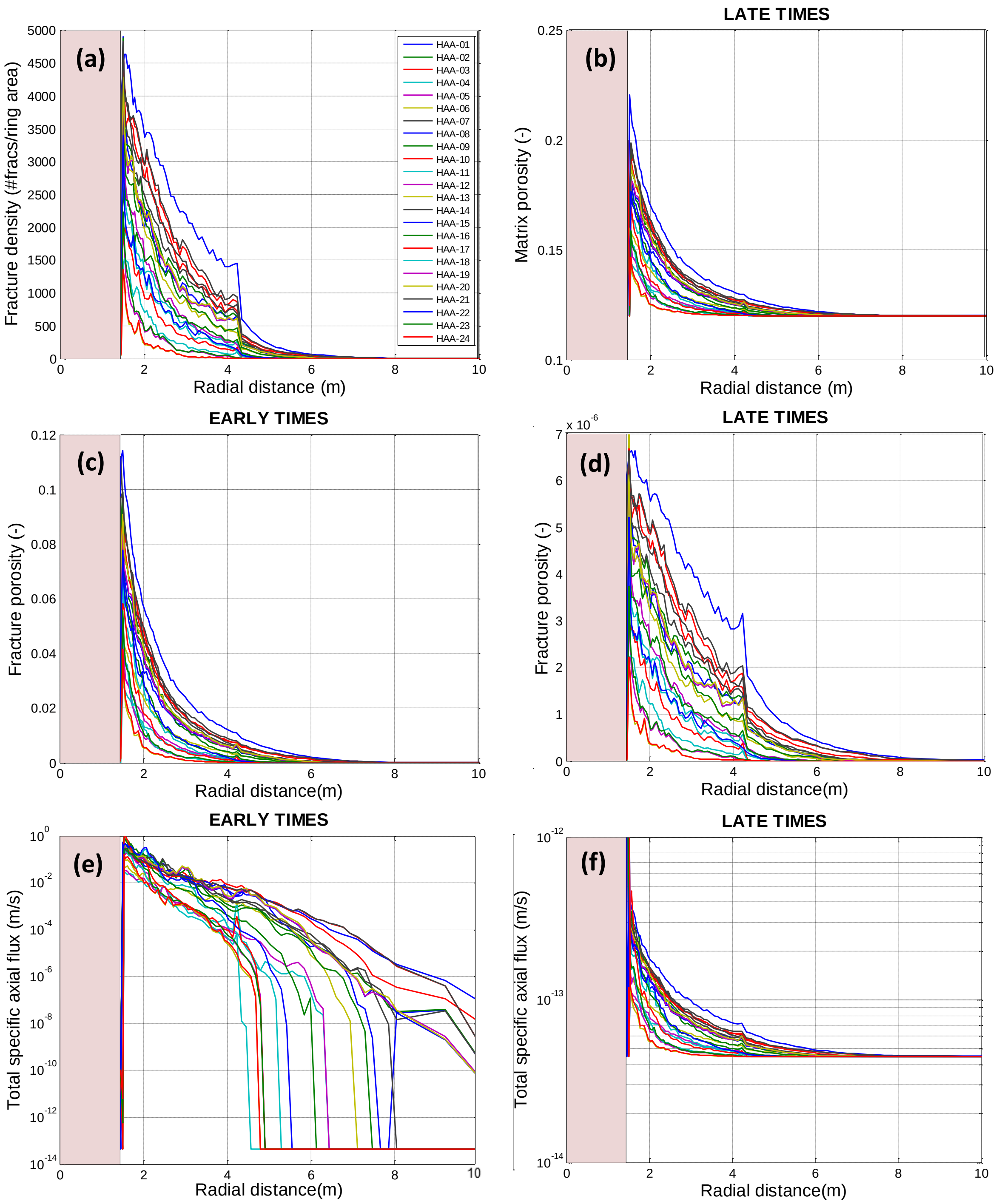

Fig. 13. Radial distribution of: (**a**) Fracture density, (**b**) matrix porosity at late times, after full re-saturation of the system, (**c**) and (**d**) fracture porosity at early times after excavation and at late times respectively, (**e**) and (**f**) total specific axial fluxes at early and late times. The pink insets depict the buffer and liner zone.

Figure 13 displays the results of the sensitivity analysis. Figure 13a displays the radial distribution of fracture density, defined as the number of fractures within a given shell of mesh cells normalized by the area of the shell. The number of fractures close to the liner depends greatly on stress conditions and strength parameters under which the FDEM simulation was generated. However, a characteristic common to all FDEM simulations is that fracture density drops dramatically to almost negligible values at radial distances greater than ~4 m (radial distances are always measured with respect to the centre of the gallery). The total extension of the EDZ (i.e., zero fracture density) is almost the same for all FDEMs, ~8 m. Figure 13b displays the spatial distribution of matrix porosity after full re-saturation of the system. Swelling of the clay rich materials forming the matrix increases matrix porosity from its initial value (0.12; Table 1) to values larger than 0.2. As observed, the sensitivity of matrix porosity to different stress/strength conditions is large close to the liner. Yet, the overall sensitivity of matrix porosity is low at a radial distance of 2 m, even if fracture densities are still high. Figures 13c and d depict the fracture porosity at early and late times. Initial fracture porosities are high, up to 0.12, but drop drastically (more than 5 orders of magnitude) after full re-saturation of the system. The sensitivity of fracture porosity to stress/strength conditions and other factors defining the repository settings is also low. The same conclusion becomes apparent from Figures 13e and f, reporting on total specific fluxes. The very high initial transmissivity of the EDZ generates axial fluxes of up to 1 m/s (assuming unit gradient conditions). These drop substantially more than 12 orders of magnitude after re-saturation of the system due to mechanical closure of the fractures and swelling of the clayey matrix. Overall, the sensitivity of the hydraulic behaviour of the EDZ to repository depth, in-situ stress conditions, rock mass strength and tunnel support system is low. The same conclusion can be drawn from Figure 14, which displays the homogenized equivalent properties of the EDZ. As observed, the radius of the EDZ is 5 to 6 m regardless of repository settings.

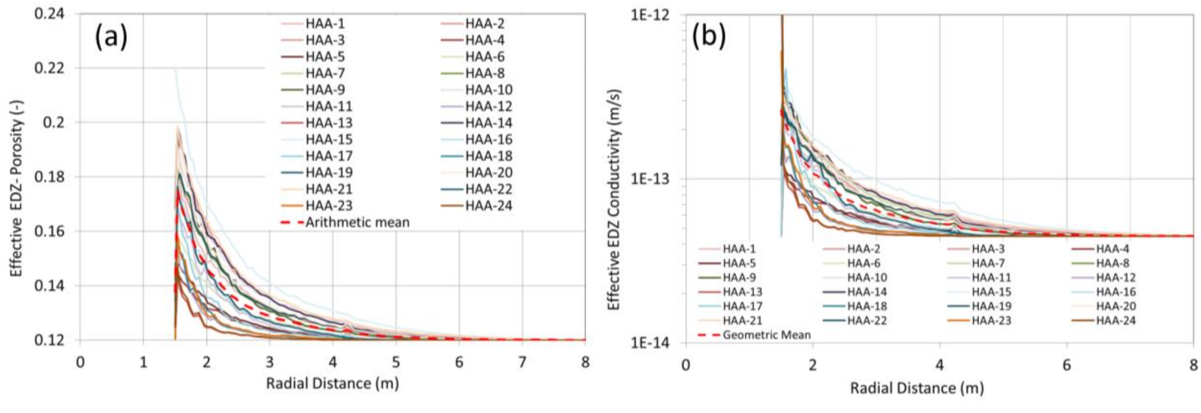

Fig. 14. Spatial distribution of equivalent porosity ϕ_{equiv} and equivalent hydraulic conductivity K_{equiv} for a variety of cases involving different repository depths, in-situ stress conditions, rock mass strengths and tunnel support systems.

Application to the HG-A experiment

The suggested approach is benchmarked with a data set from the HG-A experiment, an in-situ self-sealing experiment at the Mont Terri Underground Rock Laboratory (URL) in Switzerland. A 1 m-diameter, 13 m-long microtunnel was excavated during February 2005 using a steel augur from a niche in Gallery 04 of the URL. The microtunnel was excavated parallel to the strike of bedding planes dipping at about 50°, thus replicating the expected relationship between bedding and emplacement tunnel orientation in a deep repository (Nagra 2002). The first 6 meters of the microtunnel were lined with a steel casing immediately after excavation to stabilize the opening. The gap behind the liner was then cement-grouted, but not sealed. A purpose-built hydraulic megapacker (diameter 940 mm and sealing section length 3000 mm) was installed in 2006. The sealing section was located at 6–9 m with a 1 m grouted zone containing the non-sealing part of the packer and retaining wall from 9–10 m. The final 3 m of the microtunnel from 10–13 m form the test section which was instrumented and backfilled prior to megapacker emplacement (Fig. 15a; see Lanyon et al. 2014 for further details).

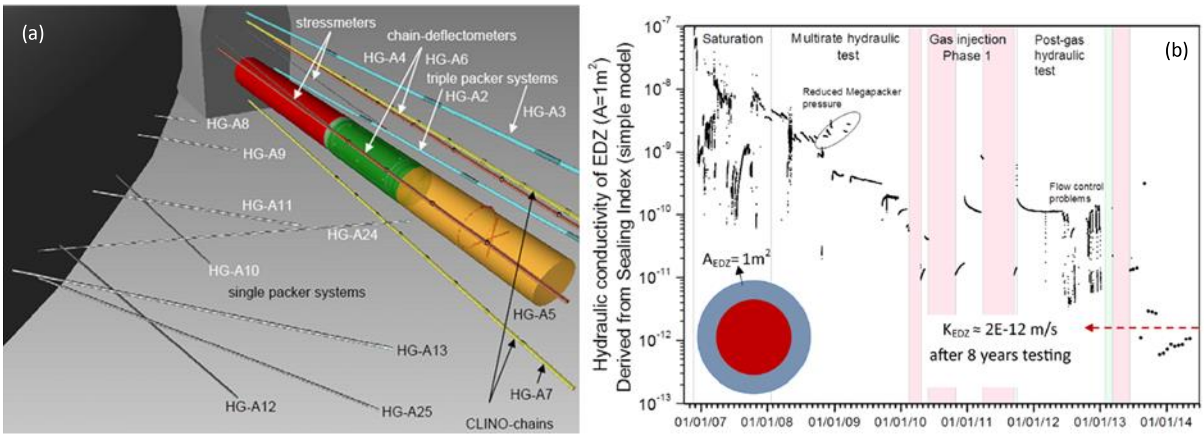

Fig. 15. (**a**) Layout and borehole instrumentation (colour coding refers to the steel liner, red; the seal section, green; and the backfilled test section, orange); (**b**) Sealing index observed during the HG-A experiment. A significant reduction in the ability to inject water into the Test Section caused by the reduction of the EDZ conductive features is observed. At the end of the observation period, the effective hydraulic conductivity of an equivalent double shell EDZ model with a cross-sectional area of 1 m^2 is around $2{\cdot}10^{-12}$ m/s.

Following emplacement of the megapacker a year-long saturation period was followed by extensive multi-rate injection testing over 2 years. Water was injected into the test section at the end of the micro-tunnel. During the multi-rate test the injection rate was reduced from an initial 10 ml/min to less than 0.1 ml/min as the permeability of the EDZ dropped. The Sealing Index SI, a simple measure of the conductance of the EDZ, was calculated from the applied injection rate and the test section pressure and is shown in Figure 15b. Assuming linear flow and a flowpath length of 3 m (seal section), the sealing index can be converted into an EDZ conductance (m3/s) by multiplying by a factor 5·10-7 (Lanyon et al. 2009 and 2014).

The model applied for the benchmarking is slightly different to that presented in previous section. In this case, we model a vertical cross section at the seal section and the canister and buffer zones are replaced by the megapacker. Available pressure measurements during the multi-rate injection test at the packered sections of observation boreholes HG-A2 and HG-A3 (Fig. 15a) are used to infer -via least squares optimization- two calibration parameters, the closure rate α and a dampening factor β multiplying the prescribed pressure at the inner boundary condition (i.e., that caused by megapacker inflation/deflation), which mimics (a) a skin effect around the microtunnel and (b) the transfer of mechanical energy to fluid and solid phases in the vicinity of the megapacker external membrane. Two different FDEM models of the EDZ are considered, in the absence and in the presence of tectonic fractures (Fig. 16b; models HG-A and HG-A-F, respectively). The model HG-A is initially not too transmissive, as compared to HG-A-F due to its relatively low fracture density.

Figure 16a displays the pressure fits at observation borehole HG-A2 for both models. Note that the suggested modelling methodology is not aimed at obtaining good fits of available measurements for several reasons: (1) the model is 2D, whereas the reaction of the system to the re-saturation of the test section and to the inflation/deflation of the megapacker is clearly 3D (Lanyon et al. 2014) and (2) the hydraulic and mechanical responses are fully decoupled (actually, the elasto-plastic stress-strain equations are not even solved). Instead, we seek for a simple model, capable of capturing the main physical processes caused by EDZ re-saturation and well-suited to Safety Assessment. Surprisingly, such simplistic model achieves relatively good fits of available measurements (see for instance, the time period 300-400 days) and captures the main trends of the reaction measured at boreholes to the forcing term.

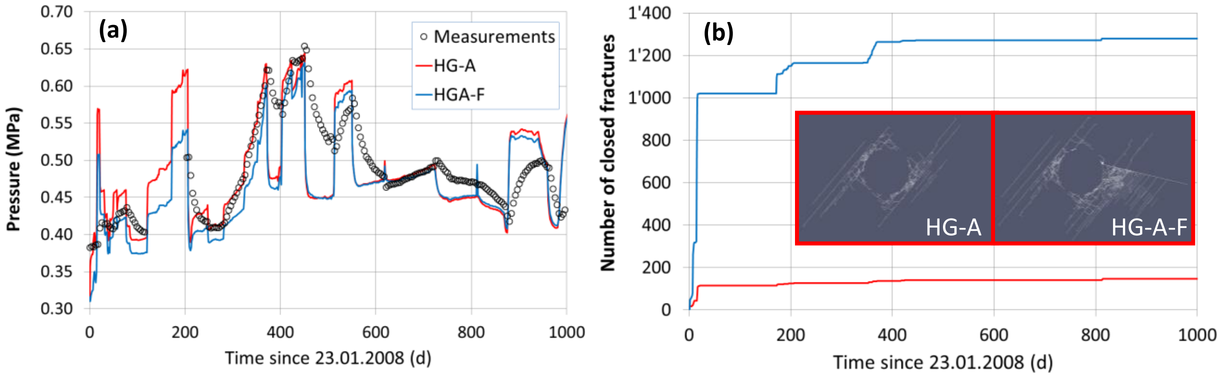

Fig. 16. (**a**) Pressure fits at observation borehole HG-A2 for simulations HG-A and HG-A-F; (**b**) number of closed fractures vs. time. In the inset, the discrete fracture networks.

Best-fitting parameters are α = 0 and β = 1 for HG-A and α = -0.35 and β = 1 for HG-A-F. The fact that a common dampening factor β is attained by the two models (i.e., in the absence and presence of tectonic imprint) reveals that the model is not much sensitive to the inner forcing term. The modelling approach can also be used to ascertain the most appropriate structural model (i.e., the characteristics of the initial FDEM). The high closure rate α for the model HG-A reveals that, even after partial re-saturation, the transmissivity of the system must be high to connect the observation points to the forcing term. Instead, the closure rate of the model HG-A-F is lower and closer to the expected values described in previous section. Therefore, the model in the presence of tectonic faults better describes the real system. These observations become apparent from Figure 16b. The high α value attained after the calibration of the model HG-A makes just a few fractures to close after partial re-saturation. Instead, the relatively low closure rate for the model HG-A-F causes most fractures to close at early times.

Hallenstrasse 10, CH-8008 Zürich
☎ +41(0)44 310 14 70
tkc@tkconsult.ch
http://www.tkconsult.ch

Conclusions

The hydraulic significance of the EDZ around the backfilled underground structures of a geological repository has been identified as an important aspect in Safety Assessments (SA). Indurated clay formations are characterised by brittle failure and complex coupled hydro-mechanical phenomena in response to the excavation process, precluding a detailed representation of the EDZ in conventional SA modelling tools. Instead, simplified models, but able to mimic the safety relevant functional features of the EDZ, are required. This work presents a heuristic sequential modelling approach, which is capable to represent adequately the key features and processes of the EDZ in indurated clays. First, brittle failure during the excavation process is simulated with a hybrid finite/discrete element code, providing realistic fracture patterns and fracture statistics, which are in broad accordance with in-situ observations. Second, EDZ self-sealing processes in response to pore pressure recovery are modelled by the interplay of hydro-mechanical fracture closure mechanisms and swelling of the intact clay matrix. Third, an abstraction towards a simplified shell-like representation of the EDZ is made. Such simple model is hydraulically equivalent to the original discrete fracture network but it is amenable to SA.

A sensitivity analysis has been carried out to assess the hydraulic significance of the EDZ for various repository settings, relevant to a deep geological repository in the proposed siting regions in Northern Switzerland. The sensitivity analysis included variations of repository depth, stress ratio, rock mass strength and design of the support system for a wide parameter range. This results in fracture patterns that exhibit marked differences in terms of size, shape and fracture density. The diversity of fracture patterns is reflected in the hydraulic simulations, which yield significantly different (several orders of magnitude) hydraulic conductances at early times of re-saturation. With time, the self-sealing of fractures takes place, causing fracture porosity and hydraulic conductivity to drop several orders of magnitude and conversely, matrix porosity and hydraulic conductivity to increase. At late times, the EDZ is restricted to a radial zone with radius 5-6m (equivalent to a thickness less than 2 tunnel diameters) for all simulation cases. A significant enhancement of hydraulic conductivity is observed only in a zone with thickness less than half of a tunnel diameter. There, the enhancement of effective hydraulic conductivity is less than 1 order of magnitude with respect to that of the intact rock matrix. Furthermore, the corresponding increase of porosity in this zone is less than 20% of the porosity of the intact rock matrix.

The methodology has been then benchmarked with a data set from an in-situ self-sealing experiment at the Mont Terri Underground Rock Laboratory (URL), demonstrating the capacity of the modelling approach to mimic the evolution of hydraulic conductance of the EDZ around a backfilled tunnel section during the re-saturation phase. The fact that a simple model (which captures the main physical phenomena behind the long-term evolution of the EDZ), reproduces well the trends observed in available measurement records should be viewed as a hopeful step in the direction of abstracting simple models, amenable to Safety Assessment, from complex representations of the EDZ.

Acknowledgements

This document is an extract is a summary of NAGRA NAB 13-94 and of a paper submitted to *GeolSoc*. This work has been supported by the Swiss National Cooperative for the Disposal of Radioactive Waste (NAGRA) and the Mont Terri Consortium, representing the partners of the HG-A experiment ANDRA (France), BGR (Germany), NWMO (Canada), NAGRA and Swisstopo (Switzerland). Special thanks to Paul Marschall (NAGRA), Andrea Lisjak, Giovanni Grasselli and Omid Mahabadi (Geomechanica), Rémi de La Vaissière (ANDRA), Helen Leung (NWMO) and Hua Shao (Federal Institute for Geosciences and Natural Resources) for reviewing this text.

References

Alcolea, A., Kuhlmann, U., Lanyon, G.W. & Marschall, P. (2014). Hydraulic conductance of the EDZ around underground structures of a geological repository for radioactive waste – A sensitivity study for the candidate host rocks in the proposed siting regions in Northern Switzerland. Nagra Arbeitsbericht NAB 13-94, Nagra, Wettingen, Switzerland.

Alheid, H.J., Aranyossy, J.F., Blümling, P., Hoteit, N. & Van Geet, M. (2007). EDZ development and evolution – State of the art. NF-PRO. Contract Number F16W-CT-2003-02389.

Aranyossy, J.F., Mayor, J.C., Marschall, P., Plas, F., Blumling, P., Van Geet, M., Armand, G., Techer, I., Alheid, A.J., Rejeb, A., Pinettes, P., Balland, C., Popp, T., Rothfuchs, T., Matray, J.M., De Craen, M., Wieczorek, K., Pudewills, A., Czaikowski, O., Hou, Z. & Fröhlich, H. (2008). EDZ Development and Evolution (RTDC 4) - Final Synthesis Report (D. 4.5.3). FP6-EURATOM/NF-PRO, F16W-CT-2003-02389.

Bernier, F., Li, X.L., Bastiaens, W., Ortiz, L., Van Geet, M., Wouters, L., Frieg, B., Blümling, P., Desrues, J., Viaggiani, G., Coll, C., Chanchole, S., De Greef, V., Hamza, R., Malinsky, L., Vervoort, A., Vanbrabant, Y., Debecker, B., Verstraelen, J., Govaerts, A., Wevers, M., Labiouse, V., Escoffier, S., Mathier, J.-F., Gastaldo, L.& Bühler, Ch. (2007). Fractures and Self-healing within the Excavation Disturbed Zone in Clays (SELFRAC). Final report, EURATOM, Fifth Framework Programme, Contract No: FIKW-CT2001-00182.

Blümling, P., Bernier, F., Lebon, P. & Martin, C.D. (2007). The excavation damaged zone in clay formations time-dependent behaviour and influence on performance assessment. Physics and Chemistry of the Earth 32(8-14), 588-599.

Bock, H., Dehandschutter, B., Martin, C.D., Mazurek, M., De Haller, A., Skoczylas, F. & Davy, C. (2010). Self-sealing of Fractures in Argillaceous Formations in the Context of Geological Disposal of Radioactive Waste Review and Synthesis Report. OECD NEA 6184. Waste Management. Paris, France: NEA OECD.

Bossart, P., Meier, P.M., Moeri, A., Trick, T. & Mayor, J.C. (2002). Geological and hydraulic Characterization of the excavation disturbed zone in the Opalinus Clay of the Mont Terri Rock Laboratory. Engineering Geology 66, 19-38.

Bossart, P. & Thury, M. (Eds). 2008. Mont Terri Rock Laboratory Project, Programme 1996 to 2007 and Results, Rep. Swiss. Geological Survey 3, Wabern, Switzerland.

Hallenstrasse 10, CH-8008 Zürich
☎ +41(0)44 310 14 70
tkc@tkconsult.ch
http://www.tkconsult.ch

Corkum, A. G. & Martin, C. D. (2007). Modelling a Mine-By test at the Mont Terri rock laboratory, Switzerland. International Journal of Rock Mechanics and Mining Sciences, 44(6), 846–859. doi:10.1016/j.ijrmms.2006.12.003.

Ferrari, A., Favero, V., Manca, D. & Laloui, L. (2013). Geotechnical characterization of core samples from the geothermal well Schlattingen SLA-1. Nagra Arbeitsbericht NAB 12-50, Nagra, Wettingen, Switzerland.

Geomechanica (2013). Extent and shape of the EDZ around underground structures of a geological repository for radioactive waste – A sensitivity study for the candidate host rocks in the proposed siting regions in Northern Switzerland. Nagra Arbeitsbericht NAB 13-78, Nagra, Wettingen, Switzerland.

Geomechanica (2014). HGA experiment: numerical simulation of the EDZ formation and mechanical re-compaction process using a FDEM approach. Mont Terri Project. Technical Note TN 2014-89, St-Ursanne, Switzerland.

Hawkins, I.R., Swift, B.T., Hoch, A.R. & Wendling, J. (2011). Comparing flows to a tunnel for single porosity, double porosity and discrete fracture representations of the EDZ. Elsevier, Physics and Chemistry of the Earth 36, pp. 1990-2002.

Jackson, C.P., Hoch, A.R. & Todman, S. (2000). Self-consistency of a heterogeneous continuum porous medium representation of a fractured medium. Water Resources Research, 36(1), 189.

Lanyon, G. W., Marschall, P; Trick, T; de la Vaissière, R, Shao, H. & Leung, H. (2009). Hydromechanical Evolution And Self-Sealing of Damage Zones Around a Microtunnel In a Claystone Formation of the Swiss Jura Mountains. In 43rd U.S. Rock Mechanics Symposium & 4th U.S. - Canada Rock Mechanics Symposium, June 28 - July 1, 2009, Asheville, North Carolina, Pages 652-663, paper 09-333.

Lanyon, G.W. & Senger, R. (2011). A Structured Approach to the Derivation of Effective Properties for Combined Water and Gas Flow in the EDZ, Transp. porous media, 1–18.

Lanyon, G. W., Marschall, P., Trick, T., de la Vaissiere, R., Shao, H. & Leung, H. (2014). Self-sealing experiments and gas injection tests in a backfilled microtunnel of the Mont Terri URL. Geological Society, London, Special Publications, 400(1), 93–106. doi:10.1144/SP400.8.

Lisjak, A., Garitte, B., Grasselli, G., Müller, H. & Vietor, T. (2015a). The excavation of a circular tunnel in a bedded argillaceous rock (Opalinus Clay): short-term rock mass response and FDEM numerical analysis. Tunnelling and Underground Space Technology, Volume 45, Pages 227–248.

Lisjak, A., Tatone, B.S.A., Mahabadi, O.K., Grasselli, G., Marschall, P., Lanyon, G. W., de la Vaissiere, R., Shao, H., Leung, H., Nussbaum, C. (2015b). Hybrid finite-discrete element simulation of the EDZ formation and mechanical sealing process around a microtunnel in Opalinus Clay. Submitted to Rock Mechanics and Rock Engineering.

Hallenstrasse 10, CH-8008 Zürich
☎ +41(0)44 310 14 70
tkc@tkconsult.ch
http://www.tkconsult.ch

Marschall, P., Distinguin, M., Shao, H., Bossart, P., Enachescu C. & Trick, T. (2006). Creation and evolution of damage zones around a microtunnel in a claystone formation of the Swiss Jura Mountains, International Symposium and Exhibition on Formation Damage Control, SPE-98537-MS.

Martin, C.D. (1997). Seventeenth Canadian Geotechnical Colloquium: The effect of cohesion loss and stress path on brittle rock strength. Canadian Geotechnical Journal 34(5), 698-725.

Martin, C.D. & Lanyon, G.W. (2003). EDZ in clay shale: Mont Terri. Mont Terri Techn. Rep.2001, 1. With contributions from P. Bossart and P. Blümling.

Nagra (2002). Projekt Opalinuston – Synthese der geowissenschaftlichen Untersuchungsergebnisse. Entsorgungsnachweis für abgebrannte Brennelemente, verglaste hochaktive sowie langlebige mittelaktive Abfälle. Nagra Technical Report NTB 02-03. Wettingen, Switzerland.

Nagra (2004). Effects of post-disposal gas generation in a repository for spent fuel, high-level waste and long-lived intermediate level waste sited in Opalinus Clay. Nagra Technical Report NTB 04-06, Nagra, Wettingen, Switzerland.

Nussbaum, C., Bossart, P., Amann, F. & Aubourg, C. (2011). Analysis of tectonic structures and excavation induced fractures in the Opalinus Clay, Mont Terri underground rock laboratory (Switzerland). Swiss Journal of Geosciences, 104(2), 187–210. doi:10.1007/s00015-011-0070-4.

Romero, E. & Gómez, R. (2013). Water and air permeability tests on deep core samples from Schlattingen SLA-1 borehole. Nagra Arbeitsbericht NAB 13-51. Nagra, Wettingen, Switzerland.

Steiner, W., Kaiser, P.K. & Spaun, G. (2010). Role of brittle fracture on swelling behaviour of weak rock tunnels: hypothesis and qualitative evidence. Geomechanics and Tunnelling 3, No. 5.

Tsang, C.F., Bernier, F. & Davies, C. (2005). Geohydromechanical processes in the Excavation Damaged Zone in crystalline rock, rock salt, and indurated and plastic clays—in the context of radioactive waste disposal. International Journal of Rock Mechanics and Mining Sciences 42(1), 109-125.

Yong, S. (2008). A three-dimensional analysis of excavation-induced perturbations in the Opalinus Clay at the Mont Terri Rock Laboratory. PhD Thesis, ETH Zurich.

Yong, S., Kaiser, P.K. & Loew, S. (2010). Influence of tectonic shears on tunnel-induced fracturing. International Journal of Rock Mechanics and Mining Sciences, 47: 984-907.

Hallenstrasse 10, CH-8008 Zürich
☎ +41(0)44 310 14 70
tkc@tkconsult.ch
http://www.tkconsult.ch